Bio-Design and Manufacturing (2026) 9:182–196
https://doi.org/10.1631/bdm.2500187

RESEARCH ARTICLE

Exploring the design potential of iridescent Flavobacteria for thermochromic engineered living materials

Clarice Risseeuw[1] · Likhitha Kummetha[2] · Colin Ingham[3] · Elvin Karana[1] · Marie-Eve Aubin-Tam[2] · Joana Martins[1]

Received: 16 April 2025 / Accepted: 18 July 2025

Abstract

By leveraging the unique qualities of microorganisms, engineered living materials (ELMs) offer functional and economic advantages in everyday applications along with notable ecological benefits. This study contributes to the growing field of biodesign by examining the potential of Flavobacteria for thermochromic ELMs. Many Flavobacteria, commonly found in marine environments, produce iridescent structural colorations as their colonies expand on semi-solid surfaces through gliding motility. In this study, we analyzed the effects of temperature variations on flavobacterium *Cellulophaga lytica* PLY-A2, characterizing distinct changes in colony growth and iridescent colorations at a macroscopic and microscopic scale. Using scanning electron microscopy, we investigated the relationship between iridescent color and the underlying cell-based optical structures. By providing insights into the temperature-responsive behavior of Flavobacteria, our findings highlight their potential for future thermochromic ELMs—with applications ranging from sustainable food packaging to smart textiles—while encouraging further characterization studies within biodesign research.

Graphical abstract

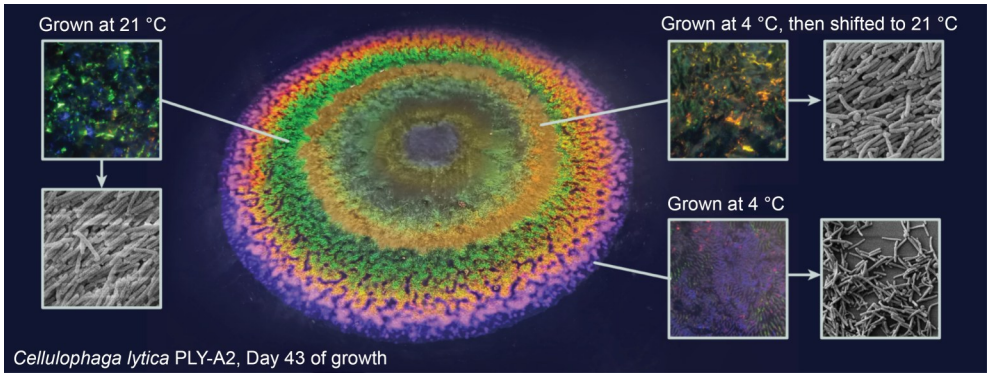

Keywords Engineered living materials (ELMs) · Living sensors · Thermochromic · Temperature-responsive · Iridescent color · *Cellulophaga lytica* PLY-A2

✉ Clarice Risseeuw
c.c.risseeuw@tudelft.nl

[1] Department of Sustainable Design Engineering, Delft University of Technology, 2628 CE Delft, The Netherlands

[2] Kavli Institute of Nanoscience, Department of Bionanoscience, Delft University of Technology, 2629 HZ Delft, The Netherlands

[3] Hoekmine BV, 3584 CS Utrecht, The Netherlands

1 Introduction

Inspired by the efficiency of natural living systems and driven by recent advances in synthetic biology and materials science, the field of engineered living materials (ELMs) has attracted substantial attention [1–5]. ELMs incorporate living cells as essential components that either construct the material itself or modulate its performance [3]. This integration can result in materials with novel functionalities, such as self-healing and biosensing, supporting a wide range of applications in healthcare, sustainable energy production, and advanced materials development [1].

In recent decades, there has been a growing interest in developing living systems in fields such as design [6–8], human–computer interaction (HCI) [9–11], and architecture [12–14]. The integration of microorganisms as design elements presents opportunities to create products that offer novel interaction possibilities, as well as more sustainable production and end-of-life processes. Contributing to these efforts, this study explores the potential of *Cellulophaga lytica* (*C. lytica*) PLY-A2 for sustainable thermochromic living materials. In their natural environments [15], these bacteria grow at temperatures ranging from 0 °C to above 30 °C, making them suitable for monitoring human environments.

In many living color-changing materials, microorganisms exhibit dynamic changes in colorations in response to environmental stimuli, including temperature. This responsive behavior may be either inherent to the organisms or the result of genetic engineering [16]. For example, a living sensor for chemical stimuli was developed by genetically modifying bacteria to achieve high levels of control, accuracy, and robustness [17]. Alternatively, biologists, engineers, and designers have leveraged microorganisms' inherent responses to develop living color-changing materials. For instance, researchers have explored how microalgae respond to mechanical stress to develop mechanoluminescent living composites [18]. These studies highlight the advantages of unmodified biological systems over human-made alternatives in terms of sensitivity, energy efficiency, and autonomy.

When integrating microorganisms into living materials, designers must develop a thorough understanding of the complex and dynamic nature of microbial responses. This poses a challenge, as many microbial species exhibit considerable variability in their responses and are often influenced by multiple stimuli, making input–output relationships difficult to identify [19]. Characterization studies are therefore essential in biodesign, as they offer insights into how different input mechanisms affect the spatiotemporal expressions of microorganisms. Accordingly, this study provides a detailed characterization of the growth and colorations of *C. lytica* PLY-A2 colonies in response to temperature variations.

C. lytica belongs to the Flavobacteriia class, of which many strains produce structural color as bacterial cells organize into photonic crystals during growth on semi-solid surfaces, including agar plates [20, 21]. Flavobacteria's cell organization has been associated with their ability to prey on other bacteria, suggesting that their photonic properties may be a secondary effect of this behavior [22].

The iridescent colorations of Flavobacteria are easily observable and highly sensitive to environmental conditions [23, 24], sparking interest across microbiology, materials science, design, and HCI communities. Recently, Sullivan et al. [25] reported the potential of Flavobacteria's iridescent biofilm as a platform for large-scale, sustainable, structurally colored materials, offering methods for controlling their optical, spatial, and temporal properties. Researchers have also explored genetic modifications as a way to alter the structural colorations in bacterial colonies [21, 26], underscoring Flavobacteria's potential for optical ELMs, such as living sensors. Moreover, Flavobacteria have been introduced to the design and HCI communities by Groutars et al. [23], who proposed a design space of input mechanisms and potential applications for living color interfaces. Risseeuw et al. [27] expanded on this work by directly interacting with Flavobacteria through pressing, tilting, and swiping, fostering a personal and dynamic interplay between humans and microbes.

While some publications have addressed the effects of temperature on Flavobacteria, particularly the colorations of *C. lytica* (Fig. 1), the broader impact of temperature variation remained unknown. To bridge this knowledge gap, our study reports for the first time the effects of temperature variations on *C. lytica* growth and provides a detailed characterization of the resulting temporal expressions. In doing so, we aim to explore the potential of these microorganisms for thermochromic living materials.

2 Experiments

This study comprised three sets of experiments, with the second and third sets building on the findings of the first. All experiments focused on the species *C. lytica*, specifically the non-harmful PLY-A2 strain. This section outlines detailed procedures for each experiment.

2.1 Experiment 1: capturing and characterizing temporal expressions of *C. lytica* PLY-A2 in response to temperature variations

To analyze the effects of temperature variations on the growth and colorations of *C. lytica* PLY-A2, the bacteria were grown for at least two weeks in large glass Petri dishes (∅ 200 mm). Each Petri dish contained 200 mL of

marine (MAR) medium supplemented with 15 g/L agar and nigrosine pigment as a contrasting agent, as described by Groutars et al. [23]. During the incubation period, colonies were exposed to two different temperatures by placing them in a 21 °C incubator and a 4 °C refrigerator. To eliminate humidity as an influencing factor [23], the incubator was set to a relative humidity of 65%, matching the conditions inside the refrigerator. Additionally, Petri dishes were sealed with Parafilm tape to reduce moisture loss during observation.

This experiment included four groups (A–D) of replicate samples (Fig. 2a), all inoculated at the center from a plate culture using an inoculation loop, and incubated upside down to safeguard colonies from condensation. Groups A and B, consisting of three samples each, served as controls and were subjected to constant temperatures for most of the experiment. Group A was incubated at 21 °C throughout, while Group B was transferred to 4 °C after 24 h. During the first 24 h post-inoculation, all groups were incubated at 21 °C to allow the bacteria to equally adapt to the new medium. Groups C and D were alternated between the two temperatures, spending 3 d at 21 °C and 11 d at 4 °C per cycle. After two full cycles of temperature shifts, Group C remained at 21 °C (Day 31), while Group D continued undergoing temperature shifts. This approach was intended to examine whether temperature-induced responses remained visible in older regions of the colonies under both conditions. To account for potential colony disruption due to movement between storage conditions, Groups C and D were prepared with four samples each instead of three.

Every weekday, all samples were photographed using a camera (EOS 250D, Canon, Japan) mounted on a tripod, equipped with a macro lens and ring flash (Figs. 2b and 2c). The camera was positioned 50 cm from the samples and configured with an exposure time of 0.25 s, ISO 800 sensitivity, an aperture of *f*/25, and a custom white balance calibrated using a color reference card. To capture the iridescent color, each sample was photographed at incident angles of 45° and 60° (similar to the method described in [23]). Two different laser-cut bases were used, each wrapped in dark fabric to minimize reflectivity during imaging.

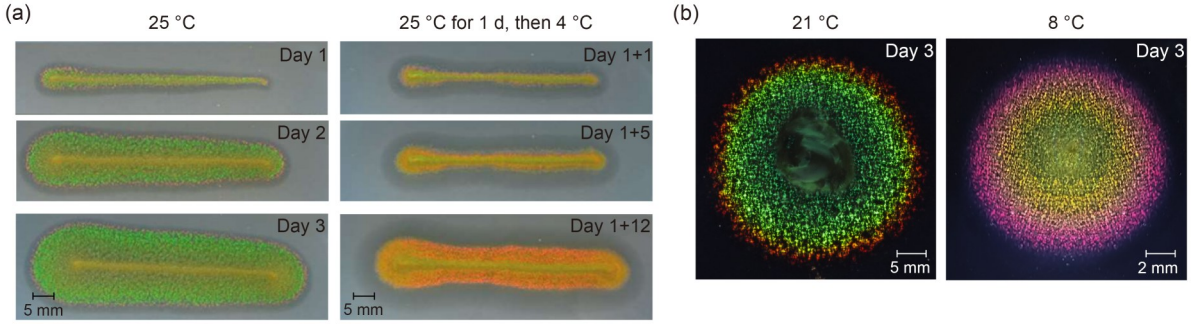

Fig. 1 Effect of temperature on the growth of *C. lytica* on solid marine medium. (a) Iridescence kinetics of a colony incubated at 25 °C (left) and a colony transferred to 4 °C after 1 d (right). Reproduced from [24], with permission from the Federation of European Microbiological Societies. (b) Structurally colored colonies grown at 21 °C (left) and 8 °C (right). Reproduced from [23], with permission from the authors

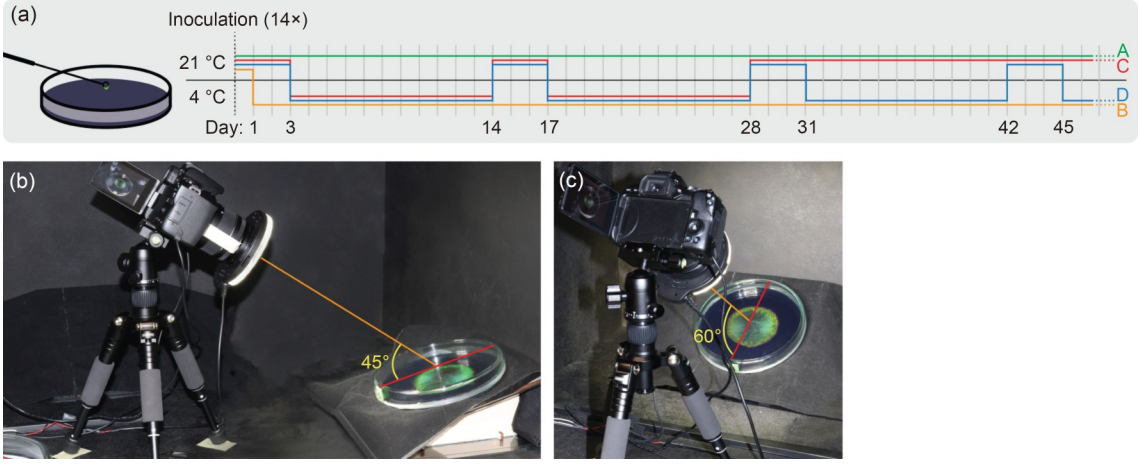

Fig. 2 Procedure for Experiment 1. (a) Timeline showing the temperature conditions over time for Groups A–D. (b, c) Image capture setup with laser-cut bases for incident angles of 45° (b) and 60° (c)

Images were examined to characterize the colony colorations in terms of texture, hue, and angle dependence, and were digitally analyzed to extract data on colony expansion rates. Although automated approaches—such as brightness thresholding [23]—were explored, accurately detecting colony surface areas was challenging due to the pointillistic edges of the colonies and color similarity to the agar medium. Consequently, each colony's radius was measured using manually placed digital markers. ArUco markers, consisting of unique binary patterns [28], were generated with a Python script and imported into Photoshop as a custom brush (Sect. S1.1 in the supplementary information). While this manual approach may have introduced some degree of human error and variability due to colonies not being perfectly circular, it provided a consistent and practical solution given the visual constraints. After image annotation, the fiducial markers were detected using a separate Python script (Sect. S1.2 in the supplementary information), allowing for the calculation and plotting of colony radii and the analysis of expansion rates across experimental groups and conditions.

2.2 Experiment 2: capturing hue homogeneity across temperature-induced color variations in *C. lytica* PLY-A2

We further analyzed the response of *C. lytica* PLY-A2 to temperature variations by examining hue homogeneity across differently colored regions. This experiment focused on the purple, orange, and green colorations induced by temperature variations, as detailed in Sect. 3.1.

Triplicate samples were inoculated and cultivated as described in Sect. 2.1, following the temperature cycling of Groups C and D (i.e., alternating between 3 d at 21 °C and 11 d at 4 °C) over a 31-d period (Fig. 3a). Macro and micro images were captured for each of the three colored regions. The purple regions were photographed after 28 d of growth, while the orange and green regions were imaged after an additional 3-d incubation at 21 °C.

For macro imaging, colonies were photographed at incident angles of 45° and 60° using the same setup described in Sect. 2.1, but from a distance of 30 cm. The resulting images were corrected for perspective distortion and masked to isolate the targeted color regions.

Additionally, the colored regions were imaged at 50× magnification to closely examine their hue characteristics (Figs. 3b–3d) using a microscope (Carl Zeiss Axio Vert.A1, Zeiss, Germany) with a camera (Sony A6100, Sony, Japan). For each colored region, three sections were excised from each colony, placed in small Petri dishes (∅35 mm), and covered with plastic foil. This setup allowed the lens to focus on the colorations, with each section being photographed three times while illuminated from the side at approximately 45° using a torch.

Macro and micro images were examined to assess the hue homogeneity of the purple, orange, and green colorations, acknowledging that the RGB capture system and interpolation process may not fully represent the true characteristics of iridescent colors. Additionally, a custom Python script (Sect. S2 in the supplementary information) was used to digitally analyze the images and plot the average hue distribution for each coloration across the different

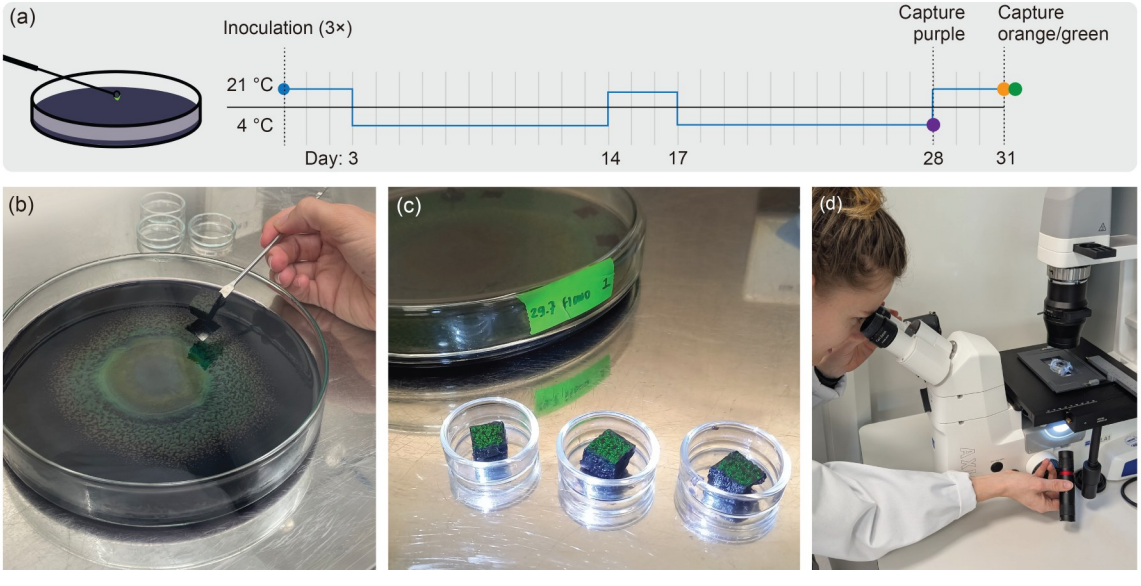

Fig. 3 Procedure for Experiment 2. (a) Timeline showing the temperature conditions over time and the image capture points for the different colorations. (b–d) Steps for capturing microscopic images of the different colored regions in *C. lytica* PLY-A2 colonies: (b) cutting sections from the colony; (c) placing the sections in small Petri dishes to position them close enough for proper lens focus; (d) observing and capturing images using the microscope

perspectives—namely, 45° and 60° incident angles for macro images, and a 90° view with side illumination for micro images.

2.3 Experiment 3: conducting SEM analysis of temperature-induced color variations in *C. lytica* PLY-A2

The underlying optical structures of the purple, orange, and green colorations in *C. lytica* PLY-A2 colonies (as detailed in Sect. 3.1) were analyzed using a scanning electron microscope (SEM), following the protocol illustrated in Fig. 4. The entire procedure was conducted twice: first, to preserve biofilms (i.e., the surface-adhered layer of cells within the colony) for the analysis of optical structures, and second, to collect loose cells from the colonies for accurate cell size measurements. This required slight modifications to the protocol, as detailed in the following paragraphs. Photographs of the SEM sample preparation process are provided in Sect. S3.1 in the supplementary information.

C. lytica PLY-A2 was cultivated in large glass Petri dishes (∅200 mm) using MAR medium [23] without nigrosine, as preliminary tests suggested that nigrosine dissolves in the fixative solution, potentially interfering with SEM analysis. Two groups of triplicate samples were cultivated, both subjected to temperature variations (Fig. 4a). The group designated for analyzing the purple region remained incubated at 4 °C until fixation on Day 31. Conversely, the group intended for analyzing green and orange regions was transferred to 21 °C for the final 3 d.

To prevent contamination, abnormal growth, or other inconsistencies that could compromise the study's validity, colonies were cultivated in triplicate. After cultivation, one representative colony was selected for each colored region to proceed with the preparation process. These colonies were placed upside down overnight, with 250 mg of

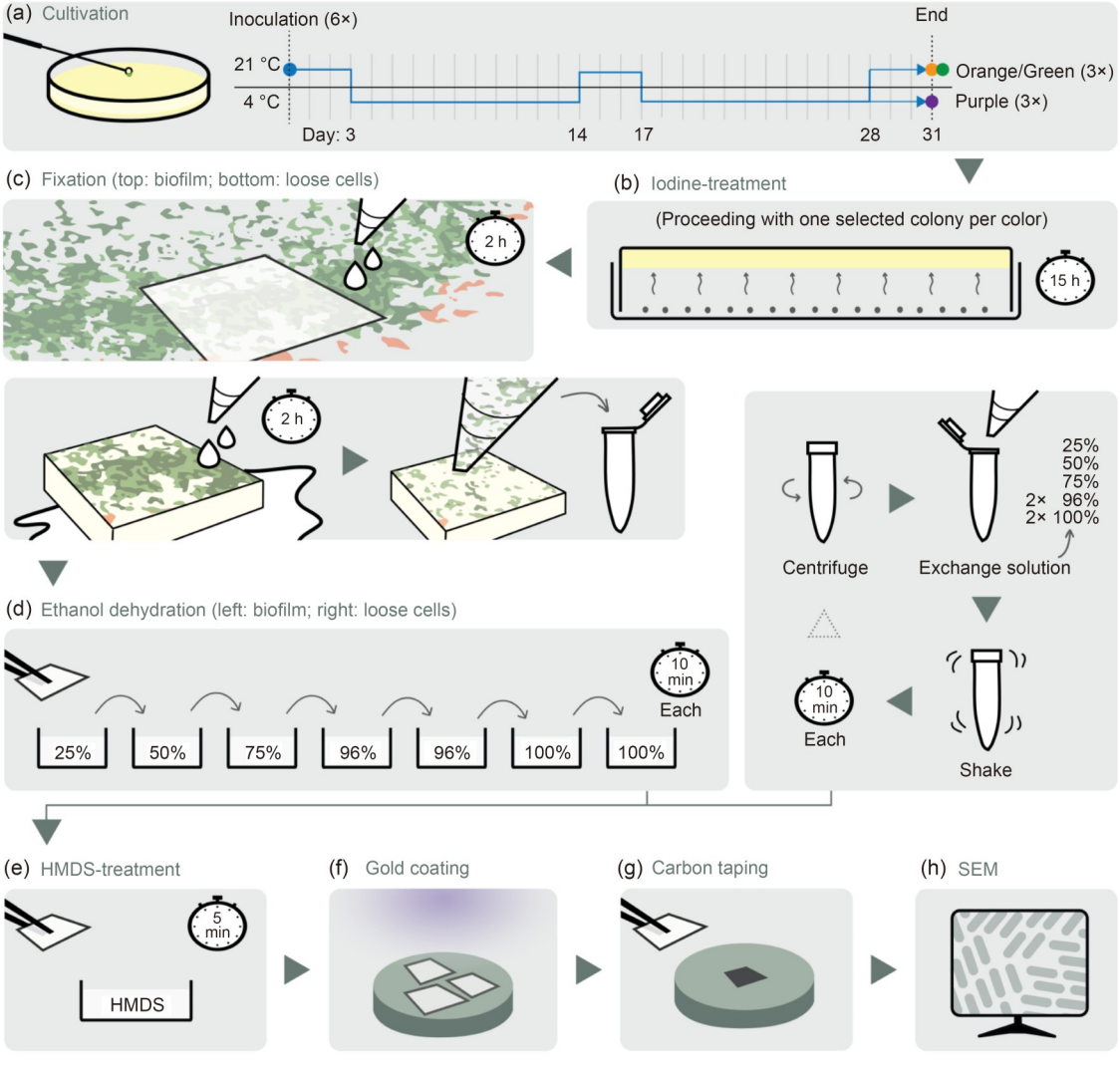

Fig. 4 Sample preparation procedure for SEM analysis: (a) cultivation; (b) iodine-treatment; (c) fixation; (d) ethanol dehydration; (e) HMDS-treatment (hexamethyldisilazane); (f) gold coating; (g) carbon taping; (h) SEM

pulverized iodine crystals in the lids of the Petri dishes (Fig. 4b), allowing iodine vapor to kill the cells without altering their optical structures [26]. During this period, the colonies selected for green and orange colorations were kept at room temperature, whereas the colony designated for the purple coloration was returned to 4 °C to prevent temperature-induced color changes. The amount of iodine crystals for this sample was increased to 500 mg to account for the reduced vapor pressure at lower temperatures. Since the iodination process temporarily alters the color of the agar medium, the colored regions were marked on the bottom of the Petri dishes with a permanent marker beforehand for easy recognition.

For SEM analysis of the biofilm, cell arrangements were preserved by placing a coverslip on top of the colony and gently pipetting a fixative solution (phosphate-buffered saline with 2% glutaraldehyde, following Refs. [25, 26]) between them (Fig. 4c, top). After 2 h, the coverslips—three per colored region—were carefully removed with the biofilm adhering to them. These coverslips were then subjected to ethanol dehydration to remove water (Fig. 4d, left) and immersed in hexamethyldisilazane (HMDS) (Fig. 4e) to prevent structural collapse during drying [29].

For SEM analysis of loose bacterial cells, three cut-outs were obtained from each colored region and submerged in the fixative solution to detach the biofilm from the growth medium in small fragments (Fig. 4c, bottom). The resulting suspension was carefully pipetted into an Eppendorf tube. Ethanol dehydration was then performed in a stepwise manner, with centrifugation before each solution change and vortexing to ensure thorough mixing with each new ethanol concentration (Fig. 4d, right). The dehydrated sample was subsequently transferred onto a coverslip before immersion in HMDS.

A gold coating was then applied to all coverslips (Fig. 4f) to establish a conductive surface, preventing charging and minimizing thermal damage during SEM imaging. The coated coverslips were mounted onto a sample holder using carbon tape (Fig. 4g) and inserted into an SEM (JSM-IT700HR, JEOL, Japan). During SEM imaging (Fig. 4h), all nine coverslips containing biofilm samples were imaged once at 1000× magnification to assess overall cell organization, and at 5000× and 10,000× magnifications at three locations each for detailed observation. Similarly, the nine coverslips with loose cells were imaged at 5000× magnification at 10 different locations to obtain sufficient data for cell size measurements.

The SEM images of loose cells were analyzed using ImageJ software, as described in [26], to determine the average bacterial cell width and length across the three colored regions. For each parameter, 150 measurements were taken, plotted as histograms, and summarized using boxplots. Differences among measurements were assessed using the nonparametric Kruskal–Wallis test. When applicable, Dunn's post hoc tests with Bonferroni correction were conducted. A p-value <0.05 was considered statistically significant.

Additionally, the optical structures observed in the SEM images of biofilms were assessed for cell alignment and homogeneity of orientation. To quantify local cell alignment in the regions visible at 5000× magnification, three SEM images were analyzed per coloration. Automated orientation analysis was hindered by low contrast between foreground and background cells, which impeded cell detection. Therefore, the orientation angles of at least 150 cells per image were manually measured in ImageJ by drawing straight lines from end to end of each cell. To focus on local cell alignment rather than overall orientation, the mean angle per image was subtracted from each measurement, resulting in relative angles. These were then plotted as histograms to compare local cell alignments among the different colorations.

3 Results

3.1 Effect of temperature variations on the temporal expressions of *C. lytica* PLY-A2

Temperature variations impacted both the expansion rate and iridescent colorations of *C. lytica* PLY-A2 colonies, consistent with previous studies that cultured *C. lytica* colonies at low or high temperatures [23, 24]. In our experiments, where temperature was varied during colony growth, we observed that temperature had a sustained effect over time, consistently influencing expansion rate and colorations in a similar manner.

Colony expansion over time was compared across the four groups (Fig. 5). Although we acknowledge that differences in the unquantified inoculum amounts may have introduced minor variations in growth rates, the data showed a clear trend: colonies grown at 21 °C expanded considerably faster than those grown at 4 °C.

In the control groups (A and B), Group A (maintained at 21 °C) expanded at a rate of 4.4 mm/d during the first 3 d but gradually slowed to about 2.3 mm/d as the colony approached the edge of the Petri dish (Fig. 5b). Conversely, Group B (maintained at 4 °C) exhibited a stable expansion rate of approximately 0.6 mm/d throughout the experiment (Fig. 5c).

Groups C and D, which were exposed to alternating temperatures, exhibited expansion rates comparable to those of the control groups during their initial 21 and 4 °C phases (i.e., Days 0–3 and 3–14, respectively) (Figs. 5b and 5c). However, their responses became more variable upon re-exposure to the same temperatures. Each time the colonies

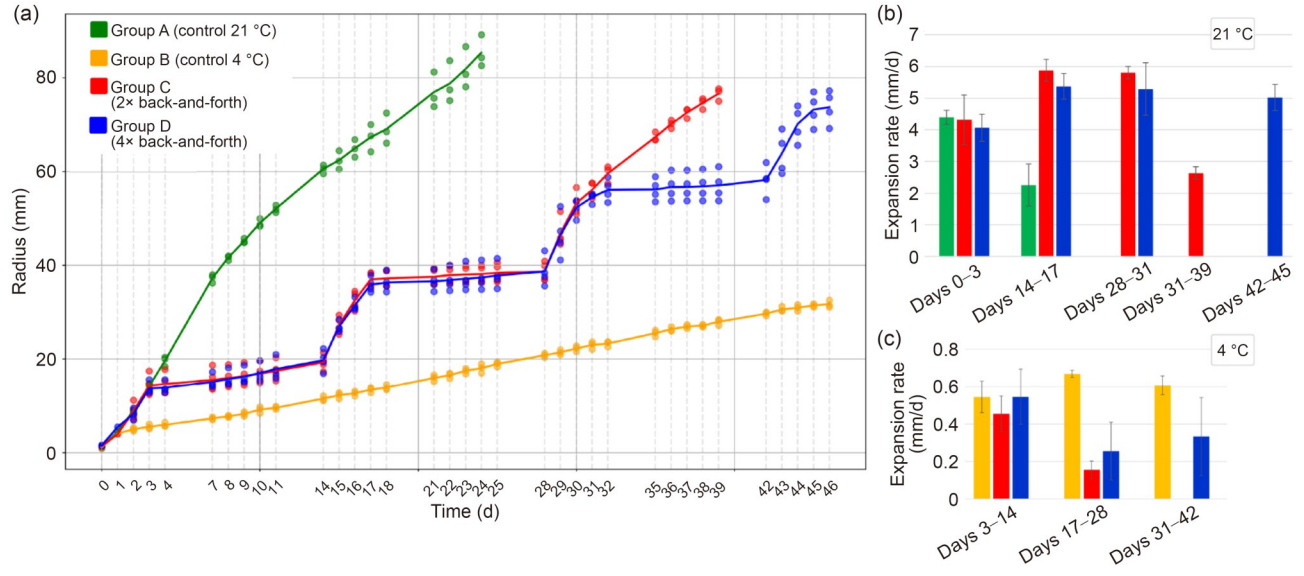

Fig. 5 Growth of colonies in control Groups A (green) and B (yellow), and in groups subjected to alternating temperatures of 21 and 4 °C, i.e., Groups C (red) and D (blue). (a) Graph showing colony radius over time with dots representing individual samples and lines indicating averages. (b, c) Graphs showing average expansion rates of each group during incubation at 21 °C (b) and 4 °C (c), with error bars indicating standard deviations (n=3 for Groups A and B; n=4 for Groups C and D)

returned to 21 °C (i.e., Days 14, 28, and 42), they expanded at rates equal to or exceeding those of Group A during its initial high-growth phase (Days 0–3) (Fig. 5b). When 21 °C conditions were sustained for a more extended period—as in Group C between Days 31 and 39—the expansion rate slowed, mirroring the pattern observed in Group A between Days 14 and 17. During the second 4 °C phase (Days 17–28), colonies in Groups C and D expanded more slowly than those in control Group B (Fig. 5c).

Colonies subjected to temperature variations over a 45-d incubation period developed distinct colored rings (Fig. 6a), as new growth consistently responded to the prevailing temperature conditions. A detailed overview of the growth patterns for replicate samples from all groups is presented in Sect. S1.3 in the supplementary information.

As shown in Fig. 6, *C. lytica* PLY-A2 colonies grown at 4 °C exhibited more intense purple hues than those grown at 21 °C, particularly when observed at an incident angle of 60° (Figs. 6b and 6c). Colonies grown at 4 °C also developed a more uniform texture in their coloration, whereas those grown at 21 °C appeared more pointillistic and scattered. When the bacteria were subjected to alternating temperatures, these temperature-induced effects became apparent in the newly formed colony regions, producing concentric rings with distinct colors and textures, as observed in Group D (Fig. 6d).

As the colonies matured and were exposed to varying temperatures, the regions that developed under different temperature conditions retained distinct color differences. While green colorations were relatively stable, purple regions were more temperature-sensitive, shifting noticeably to orange when exposed to higher temperatures (Fig. 6e), as further discussed in Sect. 3.3 and Sect. 4. Over time, although the colonies gradually lost their iridescence, differences between growth at 4 and 21 °C remained visible (Fig. 6f), indicating that the lighter colored rings preserved a record of past temperature variations.

3.2 Hue homogeneity of temperature-induced color variations in *C. lytica* PLY-A2

The hues observed across the three colored regions exhibited considerable variations, both from macroscopic and microscopic perspectives.

In the region designated as purple (Fig. 7a), cultivated at 4 °C, macroscopic images showed a color gradient ranging from orange and red hues to purple and blue near the edges when viewed at a 45° angle. At 60°, the hues shifted toward more yellow and vivid purple, as evidenced by the hue spectrum graph. Additionally, small patches of green and red were visible at both angles. Under the microscope, purple was the predominant hue, consistent with the hue spectrum graph, where hues within the purple range exhibited the highest average normalized pixel count (approximately 0.6). Although green and red hues were also observed in these microscopic images, their peak values were significantly lower (approximately 0.1). It should be noted that achieving focus on structural colorations at higher magnifications can be challenging or even unfeasible, and that the observed hues may result from clustered points of different colors rather than a uniform structural phenomenon.

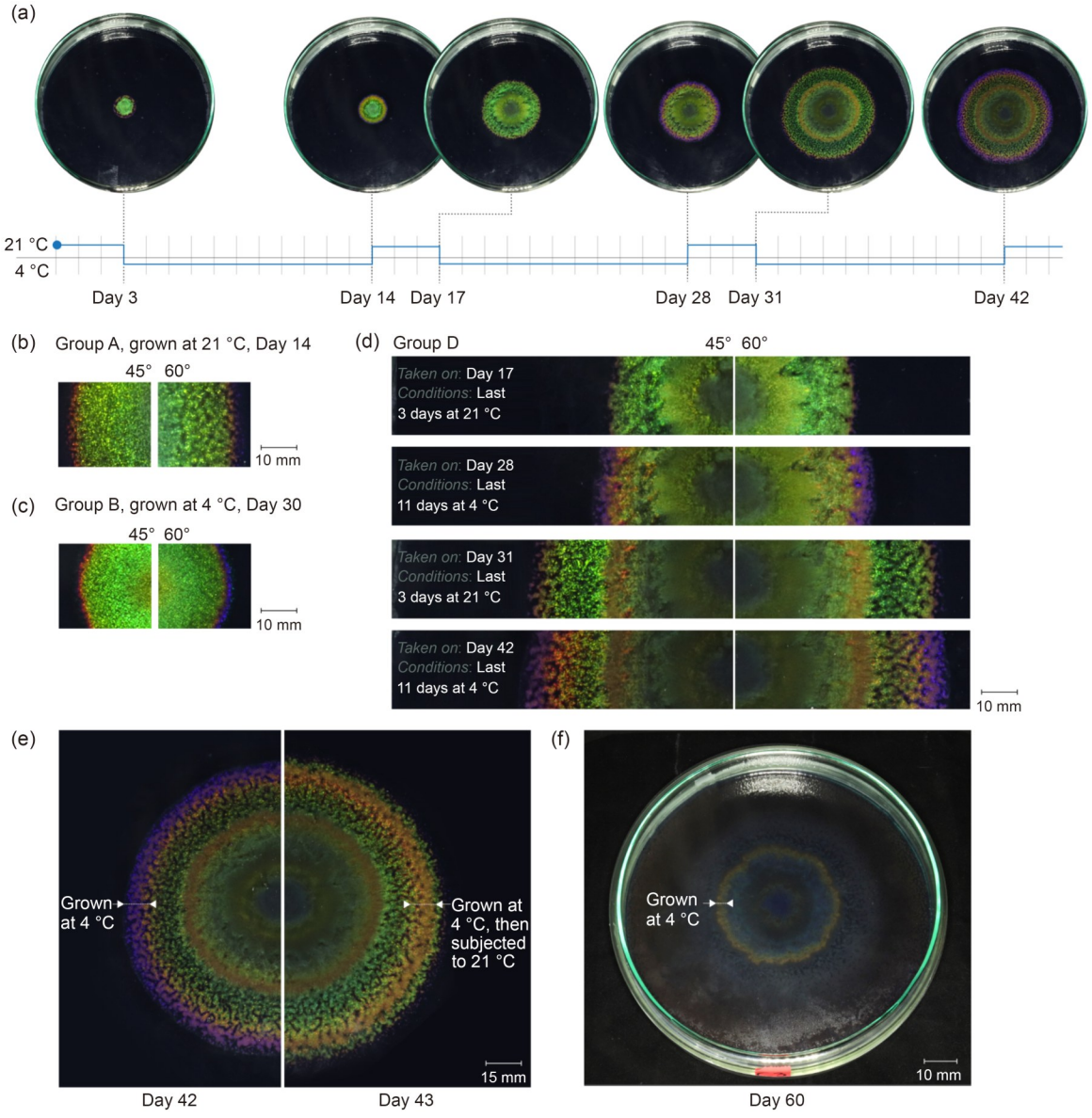

Fig. 6 Perspective-corrected images of *C. lytica* PLY-A2 colonies from Experiment 1. (a) Representative colony growth over time in Group D, subjected to temperature variations, captured at 60°, showing the formation of colored rings. (b–d) Close-ups of colony colorations captured at 45° and 60°: (b) edge of a Group A colony, grown at 21 °C for 14 d; (c) edge of a Group B colony, grown at 4 °C for 30 d; (d) multiple growth stages of a Group D colony, subjected to temperature variations, with the most recent temperature condition and duration indicated for each image set. (e, f) Temporal changes in *C. lytica* PLY-A2's colony colorations, captured at 60°: (e) representative Group D sample after 42 and 43 d, showing the transition of purple colorations (formed at 4 °C), to orange within 24 h at 21 °C; (f) group C colony on Day 60, previously subjected to temperature variations, showing loss of iridescence but retention of lighter-colored rings, possibly partially colored by the inherent yellow pigment of *C. lytica* [30]

The region designated as orange (Fig. 7b), grown at 4 °C and subsequently exposed to 21 °C, exhibited less hue variation from a macroscopic perspective, primarily displaying orange and green hues. Conversely, microscopic examination revealed a wider array of colors, including vivid orange, yellow, and various shades of green, cyan, and blue, as evidenced by the hue spectrum graph.

Finally, the region designated as green (Fig. 7c), grown at 21 °C, exhibited a color gradient at the macroscopic scale, transitioning from green and yellow to orange and red along the colony's edge. Orange hues appeared slightly more prominent at a 45° angle compared to 60°, although the overall color profile remained stable, as evidenced by the hue spectrum graph. Microscopically, numerous blue and green dots were observed, consistent with the hue spectrum graph, while red and orange dots were sparsely distributed, and too few to be represented in the graph.

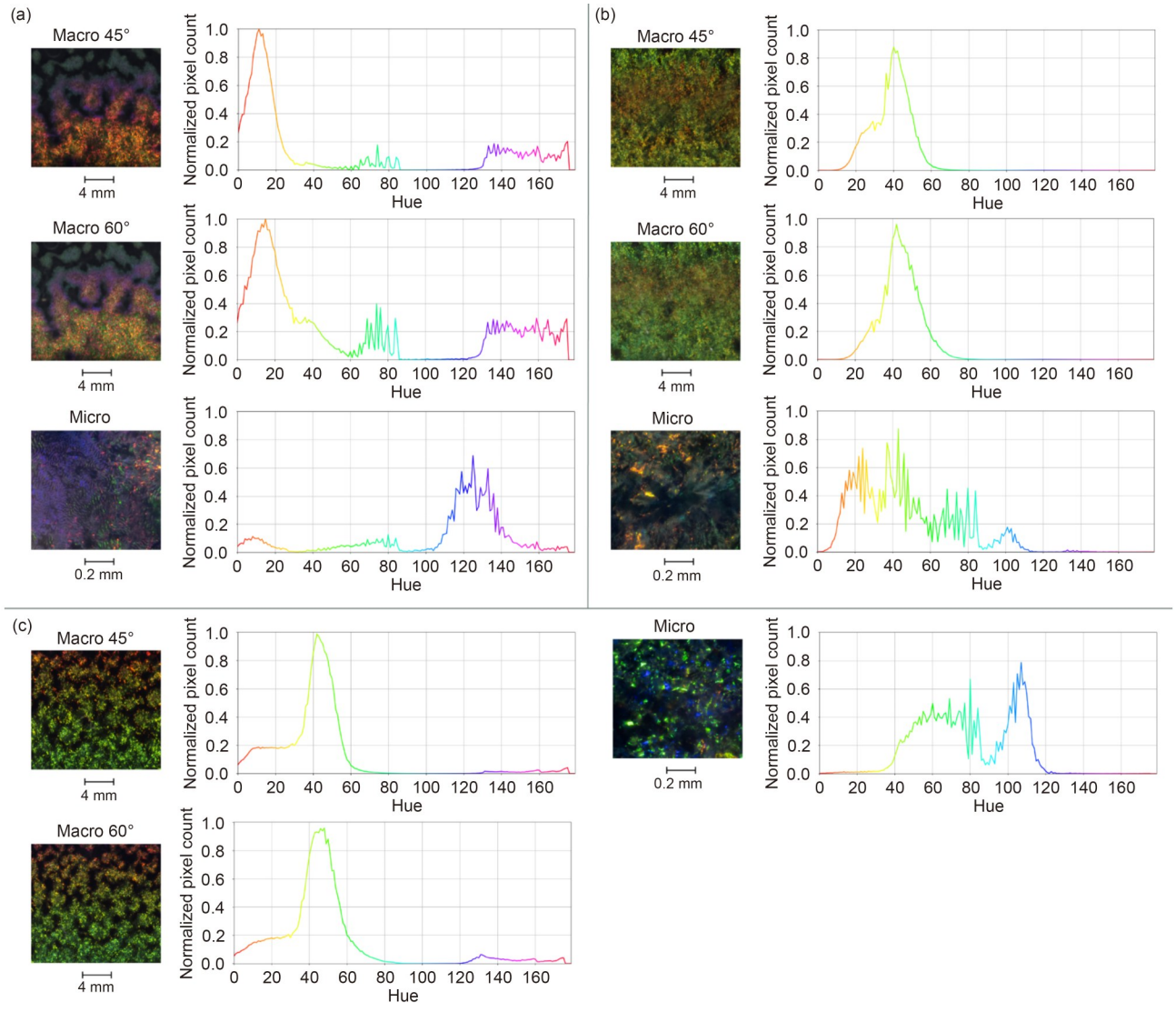

Fig. 7 Colorations of the purple (a), orange (b), and green (c) regions, shown by macroscopic and microscopic images (50× magnification), along with graphs displaying the average normalized pixel counts per hue for all images. In the macroscopic images, the edges of the colonies are positioned at the top

3.3 Relationship between temperature-induced color variations and underlying cell organization and morphology

SEM imaging revealed distinct differences in cell organization among samples from the three colored regions. In green regions, well-organized cell arrangements were clearly visible (Fig. 8a). At higher magnifications (Fig. 8a, right), tightly packed cells appeared aligned in parallel, whereas lower magnifications (Fig. 8a, left) revealed variations in orientation, resulting in circular patterns across the colony—similar to those observed in other Flavobacteria [31] (Fig. S12 in the supplementary information). Conversely, organized cell arrangements were less frequent and less structured in the orange regions (Fig. 8b) and appeared absent in purple areas (Fig. 8c).

These differences in cell alignment were further supported by the relative angle distributions (Fig. 9a). In the green regions, the relative angles showed a sharp peak, indicating consistent alignment among cells within the sampled areas. Conversely, the distributions for the orange and purple regions were broader, suggesting more variable cell orientations within the sampled areas.

Cell size measurements obtained from SEM images of loose cells (Figs. 9b–9f) revealed slight but statistically significant differences in cell length across the three colorations ($H(2) = 6.10$, $p = 0.047$) (Figs. 9b and 9c). Median lengths followed a consistent trend: cells from orange regions were the shortest (1.60 μm), followed by those in green (1.87 μm), with the longest observed in the purple regions (2.06 μm). Consistent with the boxplot (Fig. 9c), post hoc analysis revealed that cell length in the purple region

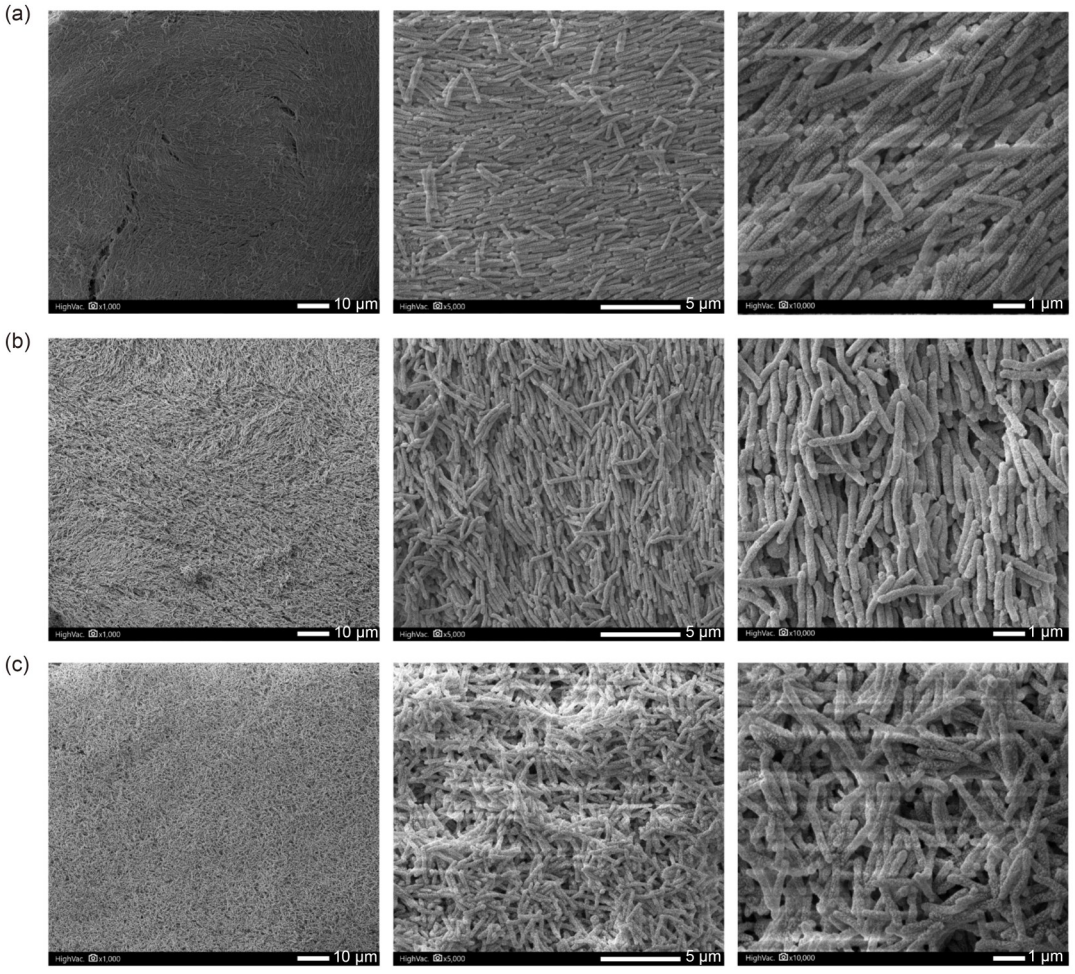

Fig. 8 SEM images of biofilms showing cell arrangements from the green (a), orange (b), and purple (c) regions, captured at three magnifications: 1000× (left), 5000× (middle), and 10,000× (right). Scale bars represent 10, 5, and 1 µm, respectively

differed significantly from the orange (p=0.014), but not from the green (p=0.17). Conversely, cell width (Figs. 9d and 9e) did not differ significantly among the colorations (H(2)=3.59, p=0.166), consistent with the substantial overlaps seen in the boxplot (Fig. 9e). Median widths showed minimal differences: green (249 nm), orange (255 nm), and purple (263 nm).

Additionally, SEM imaging of loose cells revealed the presence of spherical cells within the purple regions (Fig. 10a) and, more prominently, in the orange regions (Fig. 10b). These cells were excluded from the quantitative cell size measurements due to their atypical morphology.

4 Discussion

4.1 Reflections and limitations

This study shows that temperature variations influence the expansion rate and colorations of *C. lytica* PLY-A2, resulting in the formation of distinct colored rings within colonies. Previous research has provided explanations for structural color variations in Flavobacteria. For example, green colorations observed in *Flavobacterium* IR1 (cultivated at 25 °C) have been attributed to a relatively homogeneous crystalline arrangement of cells [32]. Conversely, the purple colorations in the same strain have been associated with a more disordered structure and increased average cell width ((480±25) nm) compared to green regions ((400±20) nm) [33]. However, in that case, both colorations developed at 25 °C, and the shift to purple was triggered by the presence of polysaccharides (fucoidan), rather than temperature variations. Similarly, another study reported notable differences in cell width between the green and red colorations of *C. lytica*'s DSM 7489 (310 nm vs. 428 nm), although these shifts occurred in response to salinity variations [25], with temperatures ranging from ambient to 27 °C. While these studies involved different strains and environmental factors to induce color changes, the reported differences in the average cell width between color variants were substantially greater than the

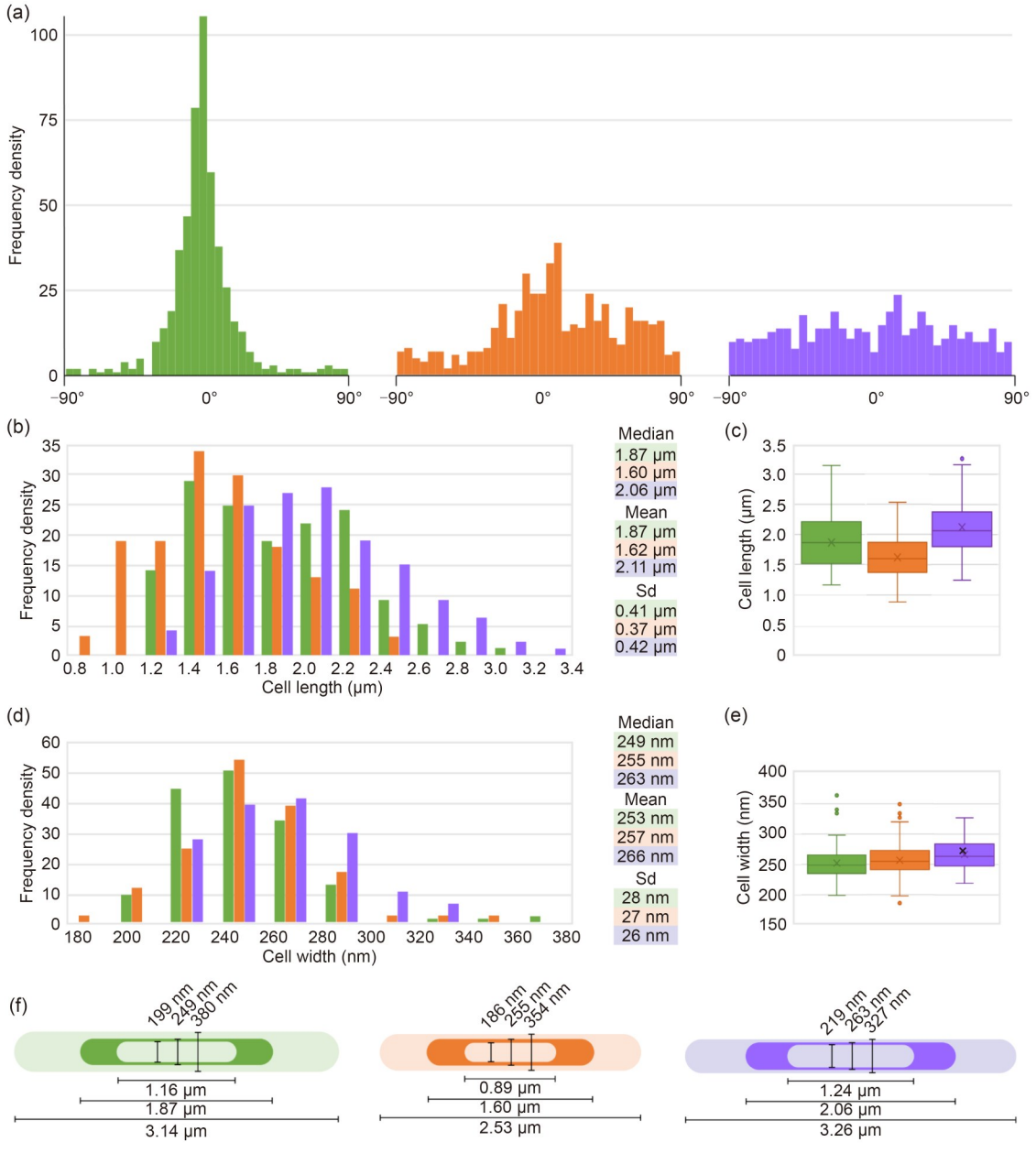

Fig. 9 Cell alignment and dimensions across the different colorations. The colors used in this figure (green, orange, and purple) correspond to the visually observed colorations and are applied consistently throughout. (a) Histograms showing the relative angle distributions within sampled areas imaged at 5000× magnification, illustrating differences in local cell alignment among the three colorations. (b, c) Histogram and corresponding boxplot of cell length measurements. (d, e) Histogram and corresponding boxplot of cell width measurements. The boxplots show the distribution of cell sizes for each region (n=150): boxes represent the interquartile range, covering the middle 50% of data; whiskers extend to capture the majority of remaining data points; individual outliers are shown as separate dots. (f) Infographic summarizing the maximum, minimum, and median cell dimensions for the three colorations

6–14 nm variation observed in our analysis (Fig. 9). This relatively small difference in cell width suggests that temperature variations have limited impact on the cell width of *C. lytica* PLY-A2 and that cell width is unlikely to be a significant determinant of the color differences observed among temperature-induced rings. Instead, other structural characteristics, such as cell spacing and organization, may play a more prominent role.

Slight differences in cell length were observed across the colored regions, particularly between the orange and purple regions. These variations may be influenced by the cells' relative position within the colony, as the purple region is closer to the colony edge, where bacterial cells tend to exhibit more active growth. However, since cell length extends perpendicular to the plane of the two-dimensional photonic crystal lattice, it is less likely—compared to cell

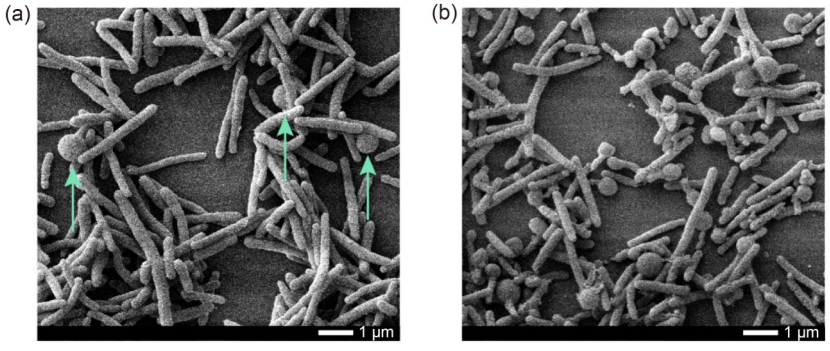

Fig. 10 SEM images showing spherical cells within the purple regions of the colony, as indicated by arrows (a), and within the orange regions (b), with scale bars representing 1 μm

width and intercellular spacing—to significantly influence the photonic interactions underlying color production in these optical structures.

SEM analysis of the biofilm was conducted to examine the underlying cell organization and better understand the origins of the distinct color differences in the temperature-induced rings. However, samples of orange and purple regions exhibited minimal or no organized cell arrangements. One possible explanation for this lack of organization is that the fixation procedure may have been less effective for the orange region and ineffective in preserving the optical structures in the purple region. This may be due to differences in cell spacing across the colored regions, with greater spacing in the purple region potentially making the optical structures more vulnerable to disruption during sample preparation. Such variations in intercellular spacing could play a crucial role in the optical mechanisms of color generation and may partially account for observed color differences across the temperature-induced rings.

The presence of spherical cells within the purple region—and more prominently in the orange region (Fig. 10)—may indicate a stress response, as bacteria are known to undergo stress-induced adaptive morphogenesis. Under unfavorable conditions, rod-shaped cells transition to a coccoid morphology [34]. Such morphological changes may influence the colorations of *C. lytica* PLY-A2 by altering the cell spacing and organization within its optical structures.

While SEM imaging offers valuable insights into cell spacing and morphology, it requires dehydration steps that may induce shrinkage, potentially affecting these measurements [32]. However, Schertel et al. [32] noted that such shrinkage tends to occur uniformly across bacterial samples, thereby preserving relative differences. Thus, despite the potential for altered absolute cell dimensions, the comparative analysis of the green, orange, and purple regions in our study remains valid. Nevertheless, future studies employing less invasive imaging techniques—such as environmental SEM and cryogenic SEM combined with goniometry [32]—could provide more accurate representations of the optical structures in Flavobacteria.

Furthermore, while RGB-based imaging in the first and second experiments provided valuable insights into the colorations of *C. lytica* PLY-A2, this approach has limitations in capturing the complexity of iridescent colors, such as their subtle spectral variations. Hyperspectral or multispectral imaging techniques, which offer higher spectral resolution, may provide more accurate characterization of the optical properties of structurally colored biofilms in future research.

Across all experimental groups, replicate samples showed strong consistency in both color expression and growth patterns (Fig. S4 in the supplementary information), highlighting the reproducibility and robustness of our findings. This consistency was evident at both the macroscopic and microscopic levels, including the emergence of concentric colored rings in response to temperature variations. Minor variations among replicates (e.g., in expansion rates; Fig. 5) likely reflect the inherent biological variability commonly associated with microorganisms.

Finally, this study shows that *C. lytica* PLY-A2 exhibits extended stability under controlled conditions, maintaining distinct and vivid color patterns for over 42 d (Fig. 6). This impressive longevity suggests the potential of temperature-responsive living materials for long-term functionality—an essential consideration for practical applications. However, the durability of these properties under real-world environmental conditions remains uncertain, as all experiments were conducted in a highly controlled laboratory setting. Transitioning to real-world applications requires a deeper understanding of how interconnected environmental factors affect the behavior of *C. lytica* PLY-A2 over time. For practical applications, thermochromic ELMs must function beyond the confines of Petri dish environments, which presents challenges related to material integration, sterility, and environmental variability. Future studies should explore strategies to enhance the resilience of Flavobacteria in applied settings, such as encapsulating bacterial colonies within protective

biomaterials. Addressing these challenges will be essential to advancing the development of thermochromic ELMs.

4.2 Implications for biodesign

The concentric colored rings formed in response to temperature variations underscore the potential of *C. lytica* PLY-A2 as a foundation for thermochromic living materials with applications across various domains.

Unlike conventional thermochromic materials, which only reflect current temperatures, these living colonies can record past temperature variations in their growth patterns, enabling the tracking of temperature history through living traces [23]. This opens up possibilities for applications where tracking past exposures is crucial, such as in the context of food safety and waste management. Additionally, these living thermochromic materials could serve as ambient temperature indicators that foster reflective engagement with environmental conditions. For instance, visualizing temperature shifts in gardens may promote awareness of the behaviors, rhythms, and interactions of other living organisms. Beyond static surfaces, these materials could be integrated into smart textiles, leveraging their dynamic color changes for temperature-responsive garments. For instance, bacteria embedded in sportswear could enable visually engaging patterns in response to body heat and ambient air, combining aesthetics and personalization with functional monitoring. In such applications, encapsulating bacteria may mitigate potential risks associated with direct contact or unintended environmental exposure.

Since *C. lytica* PLY-A2 requires minimal resources to grow—just small amounts of salt and trace nutrients—these bacteria hold promise for producing thermochromic materials in a sustainable, resource-efficient manner, as well as for temperature sensors in areas with limited electricity. Finally, given that the bacteria are unmodified, reliant on naturally derived resources, and commonly found in marine environments [15, 30], they represent an ecologically safe and biodegradable platform for developing thermochromic living materials.

While this study focused on cultivating a single strain of *C. lytica* at two specific temperatures, the potential of thermochromic living materials extends far beyond this scope. Hundreds of iridescent bacterial strains exist, each with distinct optical properties and originating from diverse environments [20]. The variability in their growth conditions and color responses could enable the customization of thermochromic living sensors tailored to specific applications and contexts.

The design applications outlined above are speculative and intended to illustrate possible future directions rather than reflect current technical feasibility. Integrating these iridescent bacteria into practical biodesign applications will require further research to address real-world constraints, including material integration, robustness, and biosafety considerations. Moreover, a more comprehensive understanding is needed of how their optical properties—such as color variability, stability, and responsiveness—are perceived and interpreted. Future work should include experiential characterization studies [35] to explore how users perceive and interact with the dynamic colorations of thermochromic ELMs. More broadly, the acceptance of ELMs poses a social challenge, closely tied to their practical context and role in everyday interactions.

5 Conclusions

This study shows how temperature variations influence the expansion rate and colorations of *C. lytica* PLY-A2. Bacterial colonies alternating between 4 and 21 °C developed concentric colored rings in orange, green, and purple, and shifted between slow and fast growth phases. The variation in color, responsiveness, and stability highlights the potential of these iridescent bacteria for thermochromic living materials. Motivated by scientific curiosity, we further explored the homogeneity of the three colored regions and their underlying optical structures. Our findings revealed that the colored regions exhibit heterogeneous hues that vary with magnification. SEM imaging showed differences in cell arrangement, potentially influenced by variations in cell spacing, while cell width remained consistent across regions, and cell length exhibited only minor variation. Spherical cells, primarily observed in the orange region and, to a lesser extent, in purple, may indicate stress responses under specific conditions. Overall, our findings underscore the promise of *C. lytica* PLY-A2 for future integration into living materials, where its dynamic colorations in response to temperature variations could pave the way for innovative thermochromic ELMs.

Supplementary Information The online version contains supplementary material available at https://doi.org/10.1631/bdm.2500187.

Acknowledgements We would like to thank the members of Materials Experience Lab and the Centre of Design Research for Regenerative Material Ecologies (DREAM) at the Department of Sustainable Design Engineering, Delft University of Technology, the Netherlands, for their feedback and support. Furthermore, we thank Evy Murraij for her explorations on temperature variations and Álvaro Escobar Doncel for inspiring our investigations into temperature-responsive growth effects. We are also grateful to our lab manager, Joren Wierenga, for his valuable discussions and support during the cultivation process of our samples. Finally, we express our gratitude to Himanshu Verma for his advice on data statistics and visualization, Kunal Masania for granting us access to his lab, and Kathrin Weiland (Momo) for assistance with the coating machine. This research received partial support from the Living Circular Labels project, funded by the Taskforce for Applied Research SIA's KIEM programme (No. CIE.06.007) in the Netherlands.

Author contributions Conceptualization: CR, EK, and JM. Formal analysis: CR and LK. Investigation: CR and LK. Methodology: CR, LK, CI, and JM. Resources: EK and MA. Visualization: CR. Writing—original draft: CR. Writing—review & editing: all authors.

Declarations

Conflict of interest The authors declare that they have no conflict of interest.

Ethical approval This study does not contain any studies with human or animal subjects performed by any of the authors.

Data availability The data that support the findings of this study are available from the corresponding author upon reasonable request.

Use of generative AI tools Generative AI tools were used to assist with computational scripting for image analysis and to support editorial aspects of the writing process, such as grammar, spelling, and clarity. All outputs were critically reviewed and revised by the authors. The AI tools did not contribute to the study design, data collection, or interpretation of results.

References

1. An B, Wang Y, Huang Y et al (2023) Engineered living materials for sustainability. *Chem Rev* 123(5):2349–2419. https://doi.org/10.1021/acs.chemrev.2c00512
2. Liu AP, Appel EA, Ashby PD et al (2022) The living interface between synthetic biology and biomaterial design. *Nat Mater* 21(4):390–397. https://doi.org/10.1038/s41563-022-01231-3
3. Nguyen PQ, Courchesne ND, Duraj-Thatte A et al (2018) Engineered living materials: prospects and challenges for using biological systems to direct the assembly of smart materials. *Adv Mater* 30(19):1704847. https://doi.org/10.1002/adma.201704847
4. Rodrigo-Navarro A, Sankaran S, Dalby MJ et al (2021) Engineered living biomaterials. *Nat Rev Mater* 6:1175–1190. https://doi.org/10.1038/s41578-021-00350-8
5. Gilbert C, Ellis T (2019) Biological engineered living materials: growing functional materials with genetically programmable properties. *ACS Synth Biol* 8(1):1–15. https://doi.org/10.1021/acssynbio.8b00423
6. Karana E, Barati B, Giaccardi E (2020) Living artefacts: conceptualizing livingness as a material quality in everyday artefacts. *Int J Des* 14(3):37–53
7. Groutars EG, Kim R, Karana E (2024) Designing living artefacts for multispecies interactions: an ecological approach. *Int J Des* 18(2):59–78. https://doi.org/10.57698/v18i2.04
8. Zhou JW, Barati B, Wu J et al (2021) Digital biofabrication to realize the potentials of plant roots for product design. *Bio-Des Manuf* 4(1):111–122. https://doi.org/10.1007/s42242-020-00088-2
9. Pataranutaporn P, Vujic A, Kong DS et al (2020) Living bits: opportunities and challenges for integrating living microorganisms in human-computer interaction. In: Proceedings of the Augmented Humans International Conference, p.1–12. https://doi.org/10.1145/3384657.3384783
10. Merritt T, Hamidi F, Alistar M et al (2020) Living media interfaces: a multi-perspective analysis of biological materials for interaction. *Digit Creat* 31(1):1–21. https://doi.org/10.1080/14626268.2019.1707231
11. Zhou JW, Kim R, Doubrovski Z et al (2023) Cyano-chromic interface: aligning human-microbe temporalities towards noticing and attending to living artefacts. In: Proceedings of the ACM Designing Interactive Systems Conference, p.820–838. https://doi.org/10.1145/3563657.3596132
12. Tyse G, Tamke M, Ramsgaard Thomsen M et al (2022) Bioluminescent micro-architectures: planning design in time, an eco-metabolistic approach to biodesign. *Archit Struct Constr* 2(4):471–479. https://doi.org/10.1007/s44150-022-00038-9
13. Andréen D, Goidea A (2022) Principles of biological design as a model for biodesign and biofabrication in architecture. *Archit Struct Constr* 2(4):481–491. https://doi.org/10.1007/s44150-022-00049-6
14. Scott J, Kaiser R, Ozkan D et al (2022) Knitted cultivation: textiling a multi-kingdom bio architecture. In: Hvejsel MF, Cruz PJS (Eds.), Structures and Architecture. A Viable Urban Perspective? (1st Ed.). CRC Press, London, UK, p.3–10
15. Kientz B, Agogué H, Lavergne C et al (2013) Isolation and distribution of iridescent *Cellulophaga* and other iridescent marine bacteria from the Charente-Maritime coast, French Atlantic. *Syst Appl Microbiol* 36(4):244–251. https://doi.org/10.1016/j.syapm.2013.02.004
16. Rivera-Tarazona LK, Campbell ZT, Ware TH (2021) Stimuli-responsive engineered living materials. *Soft Matter* 17(4):785–809. https://doi.org/10.1039/D0SM01905D
17. Liu XY, Yuk H, Lin ST et al (2018) 3D printing of living responsive materials and devices. *Adv Mater* 30(4):1704821. https://doi.org/10.1002/adma.201704821
18. Li CH, Schramma N, Wang ZJ et al (2023) Ultrasensitive and robust mechanoluminescent living composites. *Sci Adv* 9(42): eadi8643. https://doi.org/10.1126/sciadv.adi8643
19. Risseeuw C, Martinez Castro JF, Barla P et al (2023) FlavoMetrics: towards a digital tool to understand and tune living aesthetics of flavobacteria. In: Proceedings of the ACM Designing Interactive Systems Conference, p.2079–2092. https://doi.org/10.1145/3563657.3596085
20. Zomer A, Ingham CJ, von Meijenfeldt FAB et al (2024) Structural color in the bacterial domain: the ecogenomics of a 2-dimensional optical phenotype. *Proc Natl Acad Sci USA* 121(29): e2309757121. https://doi.org/10.1073/pnas.2309757121
21. Doncel ÁE, Patinios C, Campos A et al (2025) Deletion of the *moe*A gene in *Flavobacterium* IR1 drives structural color shift from green to blue and alters polysaccharide metabolism. *eLife* 14:RP105029. https://doi.org/10.7554/eLife.105029.2
22. Hamidjaja R, Capoulade J, Catón L et al (2020) The cell organization underlying structural colour is involved in *Flavobacterium*

IR1 predation. *ISME J* 14(11):2890–2900. https://doi.org/10.1038/s41396-020-00760-6
23. Groutars EG, Risseeuw CC, Ingham C et al (2022) Flavorium: an exploration of flavobacteria's living aesthetics for living color interfaces. In: Proceedings of the CHI Conference on Human Factors in Computing Systems, p.1–19. https://doi.org/10.1145/3491102.3517713
24. Kientz B, Marié P, Rosenfeld E (2012) Effect of abiotic factors on the unique glitter-like iridescence of *Cellulophaga lytica*. *FEMS Microbiol Lett* 333(2):101–108. https://doi.org/10.1111/j.1574-6968.2012.02614.x
25. Sullivan CJ, Brown K, Hung CS et al (2023) Iridescent biofilms of *Cellulophaga lytica* are tunable platforms for scalable, ordered materials. *Sci Rep* 13(1):13192. https://doi.org/10.1038/s41598-023-38797-0
26. Johansen VE, Catón L, Hamidjaja R et al (2018) Genetic manipulation of structural color in bacterial colonies. *Proc Natl Acad Sci USA* 115(11):2652–2657. https://doi.org/10.1073/pnas.1716214115
27. Risseeuw C, McQuillan H, Martins J et al (2024) (Re)activate, (Re)direct, (Re)arrange: exploring the design space of direct interactions with flavobacteria. In: Proceedings of the CHI Conference on Human Factors in Computing Systems, p.1–18. https://doi.org/10.1145/3613904.3642262
28. Garrido-Jurado S, Muñoz-Salinas R, Madrid-Cuevas FJ et al (2014) Automatic generation and detection of highly reliable fiducial markers under occlusion. *Pattern Recognit* 47(6):2280–2292. https://doi.org/10.1016/j.patcog.2014.01.005
29. Shively S, Miller WR (2009) The use of HMDS (hexamethyldisilazane) to replace critical point drying (CPD) in the preparation of tardigrades for SEM (scanning electron microscope) imaging. *Trans Kans Acad Sci* 112(4):198–200. https://doi.org/10.1660/062.112.0407
30. Pati A, Abt B, Teshima H et al (2011) Complete genome sequence of *Cellulophaga lytica* type strain (LIM-21). *Stand Genomic Sci* 4(2):221–232. https://doi.org/10.4056/sigs.1774329
31. Nakane D, Odaka S, Suzuki K et al (2021) Large-scale vortices with dynamic rotation emerged from monolayer collective motion of gliding *Flavobacteria*. *J Bacteriol* 203(14):e0007321. https://doi.org/10.1128/JB.00073-21
32. Schertel L, van de Kerkhof GT, Jacucci G et al (2020) Complex photonic response reveals three-dimensional self-organization of structural coloured bacterial colonies. *J R Soc Interface* 17(166):20200196. https://doi.org/10.1098/rsif.2020.0196
33. van de Kerkhof GT, Schertel L, Catòn L et al (2022) Polysaccharide metabolism regulates structural colour in bacterial colonies. *J R Soc Interface* 19(190):20220181. https://doi.org/10.1098/rsif.2022.0181
34. Ultee E, Ramijan K, Dame RT et al (2019) Stress-induced adaptive morphogenesis in bacteria. *Adv Microb Physiol* 74:97–141. https://doi.org/10.1016/bs.ampbs.2019.02.001
35. Camera S, Karana E (2018) Experiential characterization of materials: toward a toolkit. In: Proceedings of DRS International Conference, p.1685–1705. https://doi.org/10.21606/drs.2018.508